Soot Formation in Hydrocarbon/Air Laminar Jet Diffusion Flames

P. B. SUNDERLAND and G. M. FAETH*

Department of Aerospace Engineering, The University of Michigan, Ann Arbor, MI 48109-2118, USA

Soot processes along the axes of round laminar jet diffusion flames were studied, considering ethane, propane, *n*-butane, ethylene, propylene, and 1,3-butadiene burning in air at pressures of 25–99 kPa. Measurements included soot volume fractions, temperatures, soot structure, concentrations of major gas species and gas velocities. As distance increased along the axes of the flames, significant soot formation began when temperatures reached roughly 1250 K and fuel decomposition yielded acetylene, and ended when hydrocarbon concentrations became small at fuel-equivalence ratios of roughly 1.14. Soot growth rates were higher than earlier observations within acetylene-fueled laminar jet diffusion flames and premixed flames, which were correlated in terms of acetylene concentrations alone; this effect was attributed to either parallel soot growth channels due to the presence of significant concentrations of light hydrocarbons other than acetylene (mainly ethylene and methane) or to enhanced soot surface reactivity caused by the presence of these hydrocarbons. The present and previous soot growth data are best correlated using parallel acetylene and ethylene collision efficiencies of 0.0030 and 0.014, respectively. In contrast, present soot nucleation rates were correlated as a first-order acetylene reaction alone, with reaction parameters nearly identical to earlier findings in laminar acetylene/air diffusion flames, e.g., an activation energy of 35 kcal/gmol.

NOMENCLATURE

C_i mass of carbon per mole of species i
d burner exit fuel port diameter
d_p mean primary soot particle diameter
f fuel element mass fraction (mixture fraction)
f_s soot volume fraction
Fr burner exit Froude number, $u_o^2/(gd)$
g acceleration of gravity
$[i]$ molar concentration of species i
k Boltzmann constant
k_g soot growth rate constant
k_n soot nucleation rate constant
M_i molecular weight of species i
n reaction order
n_p number of primary particles per unit volume
p pressure
Re burner exit Reynolds number, $u_o d/\nu_o$
S soot surface area per unit volume
t time
T temperature
u streamwise velocity
$\bar{v}_i$ mean molecular velocity of species i
v_g soot growth velocity
w_g soot growth rate
w_n soot nucleation rate
X_i mole fraction of species i
z streamwise distance

Greek Symbols

η_i collision efficiency of species i
ν kinematic viscosity
ρ gas density
ρ_s soot density

Subscripts

o burner exit condition

INTRODUCTION

Soot processes are a dominant feature of hydrocarbon/air diffusion flames; they affect fundamental reaction mechanisms within the flame environment, and thus the potential for developing capabilities for computational combustion for diffusion flames, as well as an understanding of flame radiation and pollutant emission properties. Motivated by these issues, the present experimental study of the structure and soot properties of round laminar jet diffusion flames was undertaken to gain a better

* Corresponding author.

0010-2180/96/$15.00
SSDI 0010-2180(95)00182-6

COMBUSTION AND FLAME 105: 132–146 (1996)

Published by Elsevier Science Inc.

understanding of soot formation (growth and nucleation) in diffusion flames. The main objective was to extend earlier work by Sunderland and coworkers [1, 2], which was limited to soot formation in laminar acetylene/air diffusion flames, to consider other hydrocarbon fuels.

Haynes and Wagner [3], Glassman [4] and Howard [5] provide extensive reviews of past studies of soot processes in flames. There have been numerous studies of soot processes in laminar diffusion flames, involving both coflowing and opposed-jet configurations, e.g., Kent and coworkers [6–12], Santoro and coworkers [13–16], Dobbins and coworkers [17–19], Flower and coworkers [20–24], Glassman and coworkers [25–28], and references cited therein. A major limitation of these studies, however, is that soot properties and the local flame environment were not sufficiently defined for detailed consideration of soot formation processes.

Subsequent work reported in Refs. 1 and 2 undertook extensive measurements in laminar acetylene/air jet diffusion flames in order to study soot nucleation and growth. These measurements included soot volume fractions, temperatures, soot structure, concentrations of major gas species and velocities. It was found that acetylene was the dominant hydrocarbon species in the soot formation region of the acetylene/air flames, with concentrations generally 2–4 orders-of-magnitude greater than the next most abundant hydrocarbon, which was methane [2]. Soot growth rates were comparable to past observations of new soot in premixed flames [29–34]. Soot growth was first order with respect to acetylene concentration, with a negligible activation energy, yielding an acetylene/soot collision efficiency of 0.0030 after correction for effects of soot oxidation. Soot nucleation rates were correlated as a first-order acetylene reaction, with an activation energy of 39 kcal/gmol [2].

In view of this status, a major unresolved issue is the nature of soot formation processes in laminar diffusion flames involving hydrocarbon fuels other than acetylene. In particular, information is needed about the concentrations of various hydrocarbons in the soot formation region, and their impact on soot growth and nucleation. Thus, the objectives of the present study were to measure flame and soot properties in laminar diffusion flames of hydrocarbons other than acetylene burning in air, and to use these results to gain a better understanding of soot growth and nucleation. The experiments were limited to measurements along the axes of laminar jet diffusion flames at pressures of 25–99 kPa, considering ethane, propane, *n*-butane, ethylene, propylene and 1,3-butadiene burning in air.

EXPERIMENTAL METHODS

Apparatus

Two test arrangements were used for the present experiments: (1) a buoyant laminar jet diffusion flame burner operating at atmospheric pressure, identical to the arrangement of Ref. 35, that was used for weakly-sooting fuels (ethane, propane, *n*-butane, and ethylene); and (2) a weakly buoyant laminar jet diffusion flame burner operating at low pressure, identical to the arrangement of Ref. 1, that was used for strongly-sooting fuels (propylene and 1,3-butadiene).

The atmospheric-pressure burner involved upward injection of fuel from a 14.3-mm-diameter port surrounded by concentric air flow from a 102-mm-diameter port. The flow passages contained several layers of beads terminated by a honeycomb (1 mm cell size by 10 mm long) to provide a uniform flow. The flow was shielded by fine mesh screen and an outer plastic curtain in order to control drafts. Fuel and air flow rates were measured with rotameters which were calibrated by a wet-test meter. The burner assembly was traversed with a positioning accuracy of 0.1 mm in order to accommodate rigidly mounted optical instruments.

The low-pressure burner involved upward injection of fuel (or fuel/nitrogen mixtures) from a 3.3-mm-diameter port in a slow concentric flow of air. These flames burned along the axis of a vertical, windowed test chamber having a diameter and length of 300 mm. Porous plates at the top and bottom of the test chamber enclosed plenum chambers for air inflow and exhaust outflow in order to provide a uniform flow distribution over the test cham-

ber cross section. The flames were ignited with a retractable hot wire coil. Fuel and air flow rates were measured by rotameters which were calibrated by a wet-test meter. The exhaust flow was removed using a vacuum pump in conjunction with a throttling valve and bypass manifold to control the test chamber pressure. The entire test chamber could be traversed with a positioning accuracy of 0.1 mm in order to accommodate rigidly mounted optical instruments.

Instrumentation

The same instrumentation was used for both test arrangements, following Ref. 1. Soot volume fractions were found by deconvoluting laser extinction measurements for chord-like paths through the flames, similar to past work [1, 2, 13, 35]. The data were reduced assuming that soot optical properties satisfied the small-particle (Rayleigh) scattering limit, which was justified because scattering levels were small [36]. A soot refractive index of $1.57 + 0.56i$ was taken from Dalzell and Sarofim [37], similar to past work [1, 2, 13, 35], as justified by recent in situ measurements in buoyant diffusion flames [36]. Experimental uncertainties of these measurements (95% confidence) are estimated to be less than 10% for $f_s > 0.1$ ppm.

Temperatures were measured using multiline emission in regions where soot was present and using thermocouples in regions where soot was absent. The multiline emission measurements were identical to Refs. 1 and 2, and involved deconvoluting spectral radiation intensity measurements for chord-like paths through the flames. The temperatures were found from measurements at three line pairs: 600/750, 700/830, and 600/830 nm. Temperature differences between the average and any of the line pairs were less than 30 K. The thermocouple measurements involved an uncoated bare wire Pt/Pt–10% Rh junction having a diameter of 270 μm; these measurements were corrected for radiation errors. Both temperature measurements involved experimental uncertainties (95% confidence) less than 50 K [1].

Soot structure was measured using thermophoretic sampling and analysis by transmission electron microscopy (TEM), similar to earlier work [1, 2, 17, 18, 36]. The microscope used for these measurements had a 2-nm resolution. Effects of soot aggregate size cause a negligible sampling bias for present test conditions [36, 38]. As usual, soot consisted of nearly spherical and monodisperse primary particles (standard deviation of d_p less than 20% of the mean), collected into aggregates having widely varying numbers of primary particles. Primary particle diameters were measured for more than 60 particles at each location to yield experimental uncertainties (95% confidence) for d_p less than 10%. The number of primary soot particles per unit volume was then found from the other measurements, as follows:

$$n_p = 6f_s/\left(\pi d_p^3\right) \tag{1}$$

In view of the experimental uncertainties for f_s and d_p, Eq. 1 implies experimental uncertainties (95% confidence) for n_p less than 32% for $f_s > 0.1$ ppm.

Gas compositions were measured by isokinetic sampling and analysis using gas chromatography similar to past work [1, 2, 35]. A stainless-steel radiatively cooled sampling probe was used, having a port diameter of 2.1 mm. Soot coating the probe walls was periodically removed by back flushing with air. Gas species resolved by the analysis include N_2, O_2, CO_2, CO, H_2O, H_2, CH_4, C_2H_2, C_2H_4, C_2H_6, C_3H_8, C_3H_6, C_4H_{10} and C_4H_6. The gas chromatograph involved a Chromosorb 102 packed column and a 5A molecular sieve column in series, followed by a thermal conductivity detector. All H_2O was removed prior to injecting the samples into the chromatograph and H_2O concentrations were determined by assuming that the sample C/H ratio was the same as that of the fuel. For the present column arrangement, O_2 and Ar coeluted, thus, their concentrations were determined by assuming that the Ar/N ratio was the same as that of air. Experimental uncertainties (95% confidence) of these measurements were less than 15% for mole fractions greater than 100 ppm, except for O_2 where uncertainties were only less than 30% for mole fractions less than 1000 ppm due to error buildup when correcting for coelution of O_2 and Ar.

Streamwise velocities along the flame axes were measured using laser velocimetry (LV). This involved a dual-beam forward-scatter arrangement with the flow seeded with aluminum oxide particles, similar to past work [1, 2, 35]. Experimental uncertainties (95% confidence) of streamwise velocities are estimated to be less than 5%.

Test Conditions

The six test flames are summarized in Table 1. All the flames were laminar over the measurement region. The atmospheric-pressure burner was used to test the lightly-sooting fuels (C_2H_6, C_3H_8, C_4H_{10} and C_2H_4) for visible flame lengths of roughly 70 mm. These flames had fuel-port Reynolds and Froude numbers of 34–43 and 0.00064–0.0033, respectively, and were strongly buoyant, i.e., velocities increased along the axes. Radiant heat loss fractions were in the range 16.1%–25.9% of the lower heating value of the fuel (LHV), progressively increasing with the propensity of the fuel to form soot.

The low-pressure burner, operating at a pressure of 25.3 kPa, was used to test the heavily-sooting fuels (C_3H_6 and C_4H_6) for visible flame lengths of roughly 50 mm. The 1,3-butadiene fuel was diluted with nitrogen (52% nitrogen by volume in the fuel stream) in order to achieve manageable soot concentrations in the flame. These flames had fuel-port Reynolds and Froude numbers of 84–107 and 13–21, respectively, and were weakly buoyant, i.e., velocities along the axes were closely correlated with burner exit velocities over the region of interest. Radiant heat loss fractions were in the range 26.0%–29.2% of the LHV of the fuel.

RESULTS AND DISCUSSION

Flame Structure

The present study considered conditions along the axes of the flames, where mixture fractions decrease monotonically with increasing distance from the burner exit; however, present measurements generally were limited to fuel-

TABLE 1

Summary of the Test Flames

Test Flame	1[a]	2[a]	3[a]	4[a]	5[b]	6[b]
Fuel[c]	C_2H_6	C_3H_8	C_4H_{10}	C_2H_4	C_3H_6	C_4H_6
Pressure (kPa)	98.8	98.8	98.8	98.8	25.3	25.3
Burner flow (% fuel by vol.)	100	100	100	100	100	48
Fuel flow rate (cc/s)	3.38	2.00	1.52	3.36	5.31	3.20
N_2 flow rate (cc/s)	—	—	—	—	—	3.43
Air flow rate (cc/s)	269	269	269	269	710	385
Burner exit velocity (mm/s)[d]	21.4	12.6	9.5	21.3	635	793
Air velocity (mm/s)[d]	32.8	32.8	32.8	32.8	9.7	5.3
Re(−)[d]	40	40	43	34	107	84
Fr(−)[d]	0.0033	0.0011	0.00064	0.0032	13	21
Rad. heat loss (% LHV)	16.1	21.0	21.3	25.9	26.0	29.2

[a] Laminar round jet diffusion flames in air coflow with a 14.3-mm-diameter fuel port, a 102-mm-diameter air port, and a visible flame length of 70 mm.

[b] Laminar round jet diffusion flame in air coflow with a 3.3-mm-diameter fuel port, a visible flame length of 50 mm.

[c] Burner gas purities as follows: C_2H_6 (99%), C_3H_8 (99.5%), C_4H_{10} (99%), C_2H_4 (99.5%), C_3H_6 (99%), C_4H_6 (99%), N_2 (99.98%).

[d] Nominal average value based on an injection temperature of 294 K.

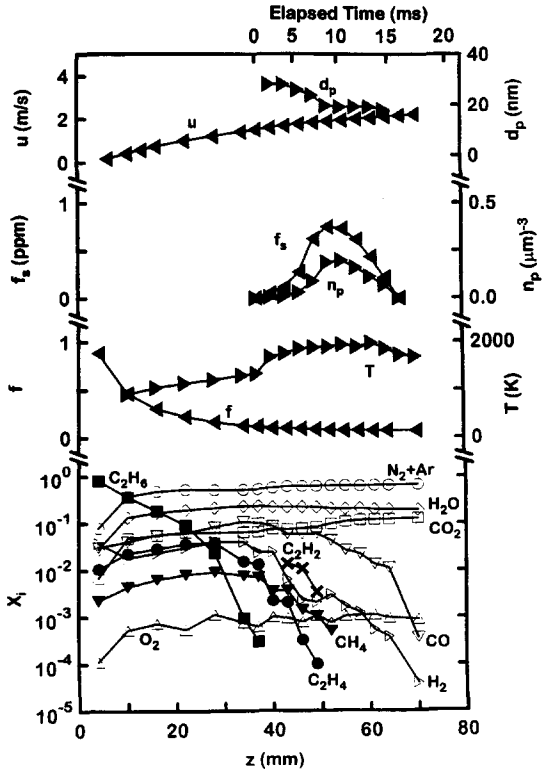

Fig. 1. Soot and flame properties along the axis of the ethane/air flame at atmospheric pressure.

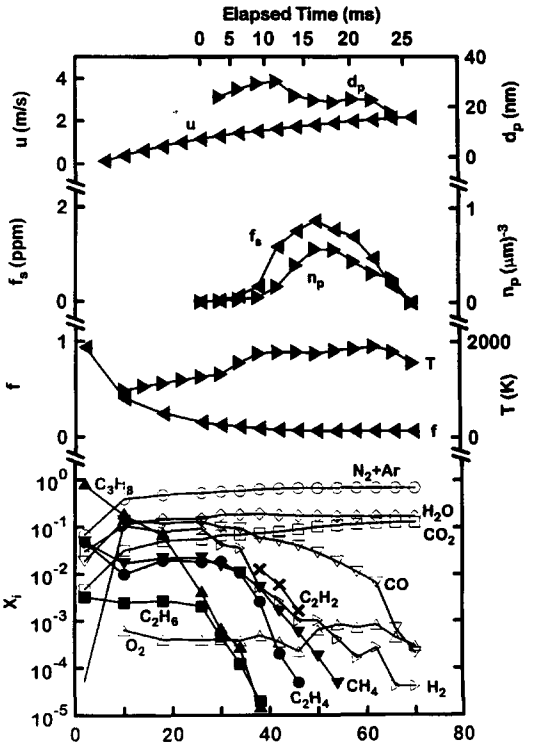

Fig. 2. Soot and flame properties along the axis of the propane/air flame at atmospheric pressure.

rich conditions, i.e., where the mixture fraction was greater than the stoichiometric mixture fraction. In addition, none of the present flames was soot-emitting. Furthermore, as noted earlier, soot structure observed during the present experiments was similar to past observations in flames [1, 2, 17, 18, 36] and consisted of nearly monodisperse spherical primary soot particles collected into polydisperse aggregates. Finally, a full tabulation of the present data can be found in Sunderland [39].

Flame and soot structure measurements along the axes of the ethane, propane, n-butane and ethylene/air flames at atmospheric pressure are illustrated in Figs. 1–4; corresponding measurements for the propylene and 1,3-butadiene-nitrogen/air flames at 25.3 kPa are illustrated in Figs. 5 and 6. Properties shown include u, d_p, f_s, n_p, f, T, and the mole fractions of major gas species, all plotted as a function of distance from the burner exit. Elapsed time, found by integrating the streamwise velocity measurements, is shown at the top of the plots; the time datum is arbitrarily set at the point where soot is first observed along the axes.

The distinction between the buoyant (Figs. 1–4) and weakly-buoyant (Figs. 5 and 6) flames is most evident from the velocity distributions: the buoyant flames exhibit a progressive increase of velocities over the range of measurements; in contrast, the weakly buoyant flames exhibit an initial velocity decrease followed by a relatively gradual velocity increase due to buoyancy.

Similar to other observations along the axes of diffusion flames [1, 2], results in Figs. 1–6 show that d_p generally reaches a maximum well before the end of the soot formation region (which roughly corresponds to the point where f_s reaches a maximum). This behavior is consistent with Tesner's [40, 41] early observation that the surface growth of soot persists to temperatures much lower than required for significant soot nucleation. As a result, the limited number of primary soot particles present near the start of the soot formation region

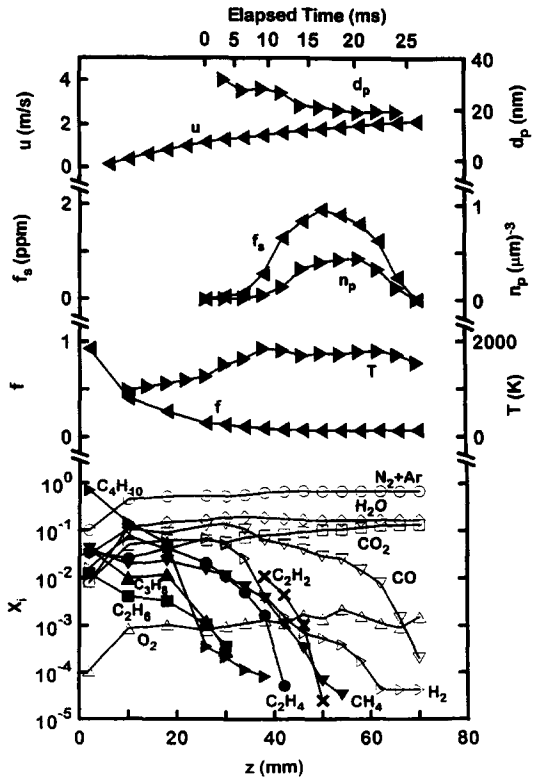

Fig. 3. Soot and flame properties along the axis of the *n*-butane/air flame at atmospheric pressure.

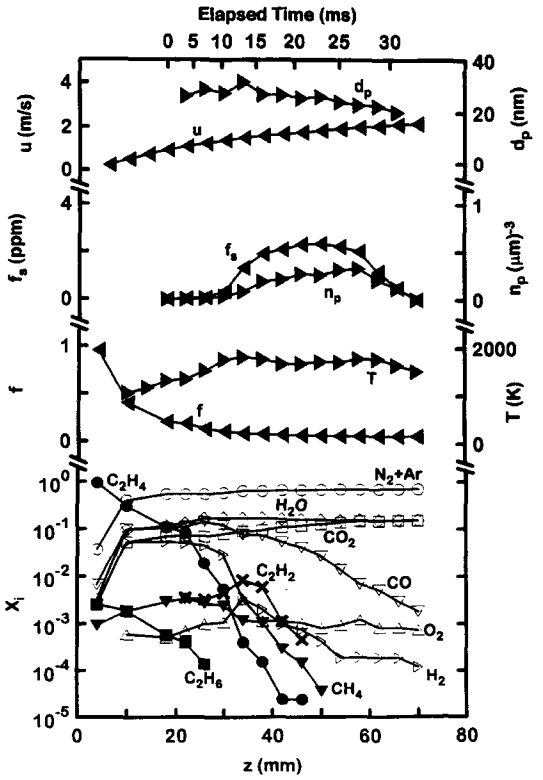

Fig. 4. Soot and flame properties along the axis of the ethylene/air flame at atmospheric pressure.

undergo rapid growth, becoming large. Subsequently, higher soot nucleation rates (evident from the rapid increase of n_p) create numerous additional primary soot particles whose shorter period of growth implies smaller values of d_p even though overall soot concentration levels continue to increase. This behavior contrasts with behavior along the soot path through the maximum soot volume fraction location in buoyant laminar jet diffusion flames, where lower nucleation rates along the path imply a closer correlation between f_s and d_p [2].

The variations of scalar properties along the axes of the present flames are qualitatively similar to earlier results for acetylene/air flames [1, 2]. Temperature reaches a broad peak before the flame tip (the point where the stoichiometric condition is reached at the axis, which generally is observed beyond the region of the data in Figs. 1–6). This behavior suggests significant effects of continuum radiation from soot. There also may be contributing effects tending to reduce temperatures within the flames due to incomplete combustion, in view of the presence of significant concentrations of CO and soot. In addition, concentrations of major gas species—N_2, O_2, fuel, CO_2, H_2O, CO and H_2—generally agree with the generalized state relationships for hydrocarbon/air flames at atmospheric pressure, proposed in Ref. 42; however, an exception is O_2 concentrations at rich conditions, where it is likely that earlier measurements were not corrected for the coelution of O_2 and Ar as discussed in Ref. 2.

The extent of the soot formation regions in Figs. 1–6 is similar to earlier observations for acetylene/air flames [1, 2]. In particular, significant rates of soot formation, evidenced by increasing f_s, are observed only when temperatures exceed roughly 1250 K, in agreement with past observations in diffusion flames [1–5]. The end of soot formation occurs when the concentrations of hydrocarbons become small, well before the flame sheet is reached, at a fuel-equivalence ratio of roughly 1.14, similar

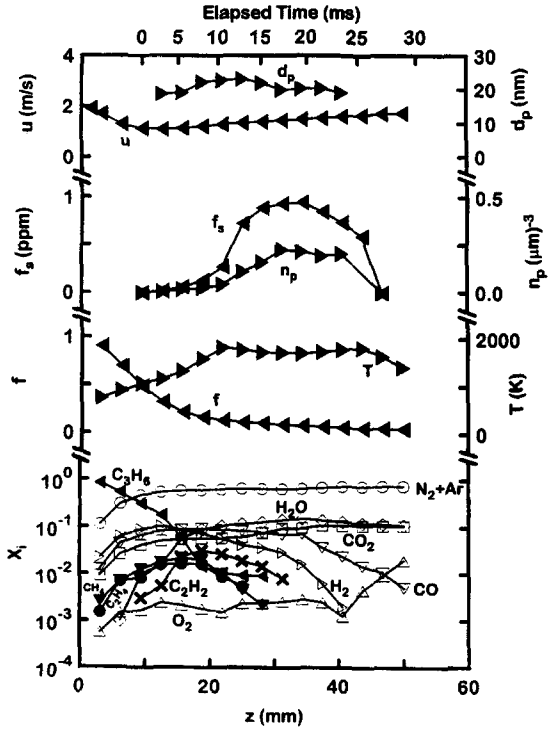

Fig. 5. Soot and flame properties along the axis of the propylene/air flame at 25.3 kPa.

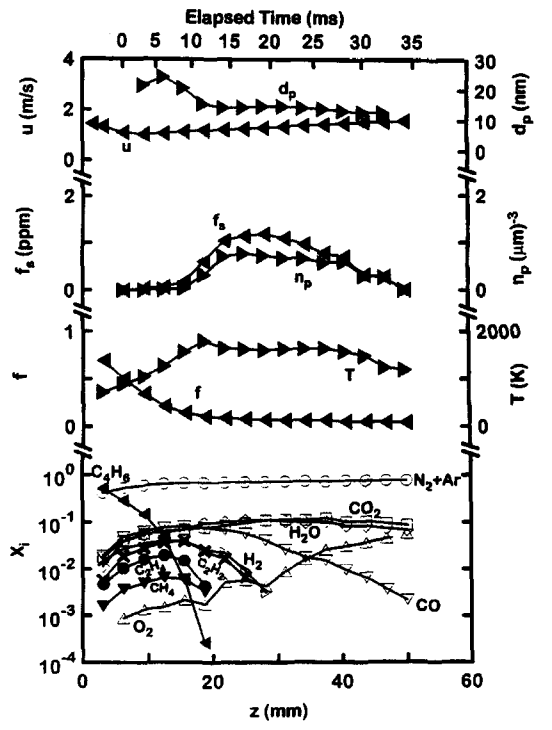

Fig. 6. Soot and flame properties along the axis of the 1,3-butadiene/air flame at 25.3 kPa.

to earlier observations in acetylene/air flames [1, 2].

The soot formation regions of the present flames contain significant amounts of light hydrocarbons other than acetylene, in contrast to the acetylene flames studied in Refs. 1 and 2. Another feature of soot formation in the present flames is that it is concurrent with soot oxidation, similar to earlier observations in acetylene/air flames [1, 2]. This is evident from the presence of soot-oxidizing species, e.g., O_2, CO_2, and H_2O, throughout the soot formation region, see Figs. 1–6. In fact, soot oxidation at fuel-rich conditions for the present flames is sufficiently fast that the soot generally disappears before fuel-lean conditions are reached along the axes. Past work [2] suggests that CO_2 and O_2 concentrations are sufficient to contribute significantly to soot oxidation at fuel-rich conditions. It also is likely that oxidation by OH becomes important toward the end of the fuel-rich region, as hydrocarbon concentrations become small and the concentrations of OH begin to increase [16, 43, 44]; unfortunately, direct measurements of OH were not obtained during the present investigation in order to establish the role of OH oxidation directly.

Soot Growth

Soot growth along the axes of the test flames was studied similar to Refs. 1 and 2. Soot surface growth, rather than nucleation, was assumed to dominate soot mass production; this approximation is plausible because primary particles become visible when they are roughly 5 nm in diameter, while primary particle diameters observed in the soot growth region generally were larger than 15 nm. Effects of soot thermophoresis and mass diffusion are small for present flames; therefore, soot was assumed to convect along streamlines at the local gas velocity. Finally, the surface area available for soot growth was found assuming that soot aggregates consist of monosized spherical particles that meet at a point. Then the gross rate of soot mass growth along a

streamline becomes [1]:

$$w_g = \rho_s v_g = (\rho/S)d(\rho_s f_s/\rho)/dt. \quad (2)$$

The soot surface area per unit volume, S, in Eq. 2 is found from [1]

$$S = \pi d_p^2 n_p = 6 f_s/d_p. \quad (3)$$

The local gas density in Eq. 2 was found from present species concentration and temperature measurements, assuming an ideal gas mixture of the major gas species and neglecting the volume of soot (which is present only at ppm levels). The soot density in Eq. 2 was taken to be $\rho_s = 1850$ kg/m^3, as discussed by Puri et al. [15] and used in earlier work [1, 2]. Finally, the temporal derivative in Eq. 2 was found from three-point least-squares fits of $\rho_s f_s/\rho$, as before [1, 2].

The net soot growth rates found from Eqs. 2 and 3, and corrected for oxidation (as discussed subsequently), are plotted as a function of distance along the axis for the six test flames in Figs. 7–12. In order to locate the soot growth region, nucleation rates for these conditions are shown on the plots as well (the method used to compute nucleation rates and the interpretation of these results will be taken up later). The onset of growth is controlled by the availability of primary soot particles and roughly corresponds to the first observations of soot nucleation. The end of the soot growth region is reached when f_s reaches a maximum along the axis, which is indicated by the last point where w_g is plotted in Figs. 7–12. Finally,

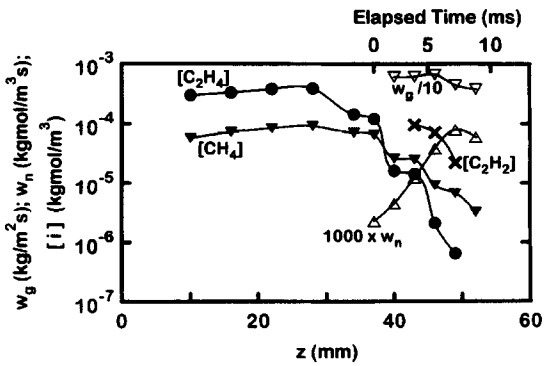

Fig. 7. Net soot growth and nucleation rates along the axis of the ethane/air flame at atmospheric pressure.

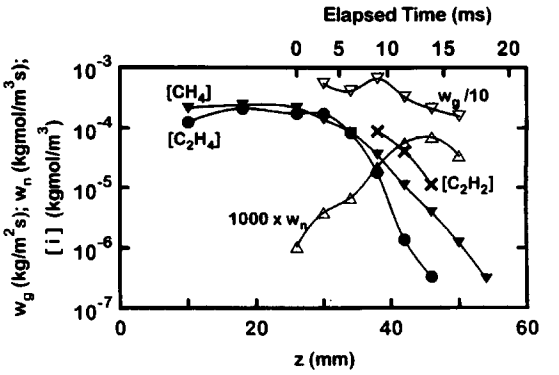

Fig. 8. Net soot growth and nucleation rates along the axis of the propane/air flame at atmospheric pressure.

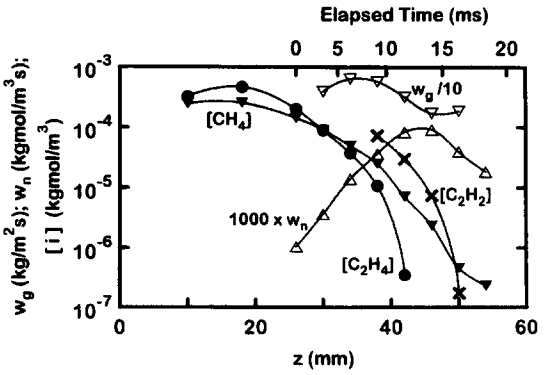

Fig. 9. Net soot growth and nucleation rates along the axis of the n-butane/air flame at atmospheric pressure.

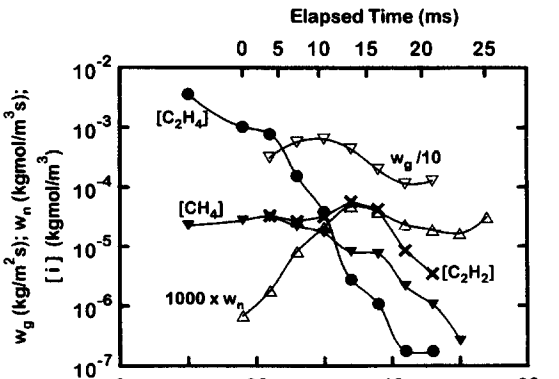

Fig. 10. Net soot growth and nucleation rates along the axis of the ethylene/air flame at atmospheric pressure.

the concentrations of the most prevalent hydrocarbons in the soot formation region—C_2H_2, CH_4, and C_2H_4—are shown on the plots in order to assist the interpretation of the growth and nucleation rate measurements.

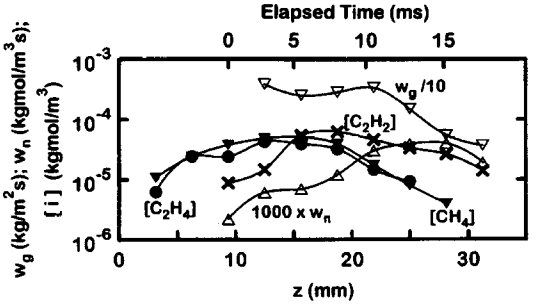

Fig. 11. Net soot growth and nucleation rates along the axis of the propylene/air flame at 25.3 kPa.

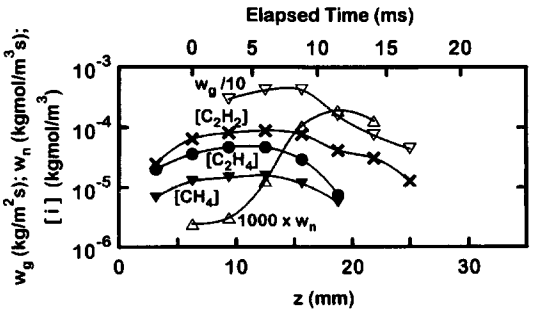

Fig. 12. Net soot growth and nucleation rates along the axis of the 1,3-butadiene/air flame at 25.3 kPa.

Net soot growth rates in Figs. 7–12 range from 10^{-3} to 10^{-2} kg/m^{2}s. Acetylene, which is correlated with soot growth in flow tubes [45–47], premixed flames [29–34], recent detailed models of premixed flames [48, 49] and acetylene-fueled diffusion flames [1, 2], is the most abundant hydrocarbon near the end of the soot growth region, which suggests that it dominates soot production at these conditions. This behavior is supported by the observation that the end of the soot growth region generally coincides with the disappearance of acetylene. On the other hand, concentrations of ethylene are comparable to or greater than those of acetylene near the start of the soot growth region, suggesting potential for the participation of ethylene in soot growth as well. Additionally, methane concentrations are intermediate between acetylene and ethylene in the soot growth region, although there is little evidence for the direct participation of methane in soot growth [45–49]. Finally, hydrogen, which is thought to be involved in the activation of carbon surfaces [48, 49], has concentrations (see Figs. 1–6) that are comparable to acetylene concentrations in the soot growth region.

In view of these observations, the first step in correlating soot growth was to associate gross growth with acetylene concentrations, similar to Refs. 1 and 2, as follows:

$$w_g = k_g(T)[C_2H_2]^n, \tag{4}$$

where $k_g(T)$ normally is an Arrhenius expression. Similar to the acetylene/air diffusion flames [1, 2], however, the temperature dependence of $k_g(T)$ was not significant and a correlation of present measurements was sought by plotting w_g as a function of the molar concentration of acetylene as illustrated in Fig. 13. Other results illustrated on this figure include measurements [1, 2] and a correlation [2] for acetylene/air diffusion flames and measurements in premixed flames [29–34]. These results all represent gross soot growth rates, uncorrected for effects of simultaneous soot oxidation.

The results illustrated in Fig. 13 suggest comparable growth rates for acetylene/air diffusion flames and for new soot in premixed flames (the uppermost data points for the premixed flames), however, the diffusion flames do not exhibit reduced growth rates with increasing soot age, typical of premixed flames [1]. Soot growth rates in the present hydrocar-

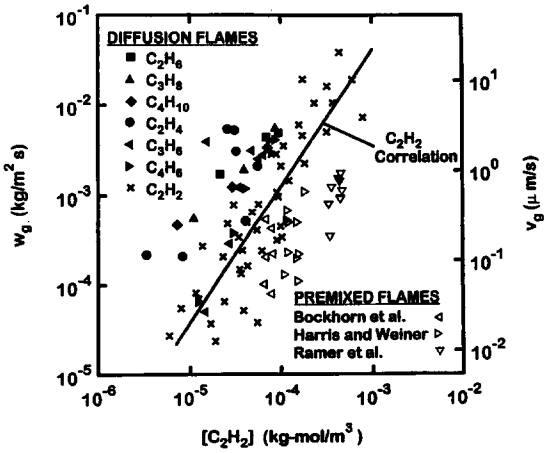

Fig. 13. Gross soot growth rates along the axes of laminar hydrocarbon/air diffusion flames, similar results for acetylene/air diffusion flames from Refs. 1 and 2, and similar results for premixed flames from Refs. 29–34.

bon/air flames are significantly higher than in the acetylene/air flames of Refs. 1 and 2, however, suggesting that significant concentrations of light hydrocarbons other than acetylene either participate in soot growth channels other than the acetylene channel, or enhance soot surface reactivity to reaction with acetylene. Although present rates of soot growth are significantly larger than the earlier results for acetylene/air flames, however, the apparent order of gross soot growth with respect to acetylene concentrations is similar, 1.11 with a standard deviation of 0.22.

Similar to results for acetylene/air flames [1, 2], the apparent order of gross soot growth with respect to acetylene concentration for the present hydrocarbon/air diffusion flames is somewhat higher than past suggestions of first-order behavior based on measurements in premixed flames [29–34]. This behavior is due to soot oxidation masking actual (net) soot growth rates, particularly when gross soot growth rates become small and oxidant concentrations become large near the end of the soot growth region. Corrections for soot oxidation were carried out in the same manner as in Refs. 1 and 2: soot oxidation by O_2 was estimated using the rate expression of Nagle and Strickland-Constable [50] which was subsequently confirmed by Park and Appleton [51]; and soot oxidation by CO_2 and H_2O was estimated following Johnstone et al. [52] and Libby and Blake [53, 54], in agreement with Bradley et al. [55]. Soot oxidation by OH, as discussed by Neoh et al. [56], was ignored because concentrations of OH are negligible in the soot formation region due to the presence of light hydrocarbon species [16, 42, 43]. Evaluation of these procedures in Ref. 1, based on observed soot oxidation rates in the fuel-lean region of acetylene/air flames, indicated significantly overestimated soot oxidation rates in agreement with Puri et al. [16]; therefore, conditions where the gross growth rate was negative were eliminated from the following results. For the present soot formation regions, reaction with CO_2 dominated soot oxidation, e.g., soot oxidation rates due to CO_2 and H_2O averaged 4 and 0.0007 times the corresponding O_2 rates.

The present net soot growth rates, corrected for soot oxidation, are plotted as a function of acetylene concentration in Fig. 14. The net soot growth rate has been plotted in a manner that anticipates a collision efficiency expression, i.e.,

$$w_{g_i} = \eta_i C_i \bar{v}_i [i]/4, \tag{5}$$

where

$$\bar{v}_i = (8kT/(\pi M_i))^{1/2} \tag{6}$$

is the (Boltzmann) equilibrium mean molecular velocity of species i. Also shown on the plot are results for acetylene/air diffusion flames from Refs. 1 and 2, corrected for effects of soot oxidation in the same manner, and results for premixed flames from Refs. 29–34 where no correction has been made for soot oxidation. When plotted in this manner, the measurements for hydrocarbon/air flames indicate behavior compatible with a first-order acetylene reaction within statistical significance, but with generally higher net soot growth rates than the results of Refs. 1 and 2 for acetylene/air flames. The increased net growth rates can be quantified by an average collision efficiency from Eq. 5, attributing all net soot growth to a first-order acetylene reaction. This yielded an acetylene collision efficiency of 0.011 with an uncertainty (95% confidence) of 0.004 for the

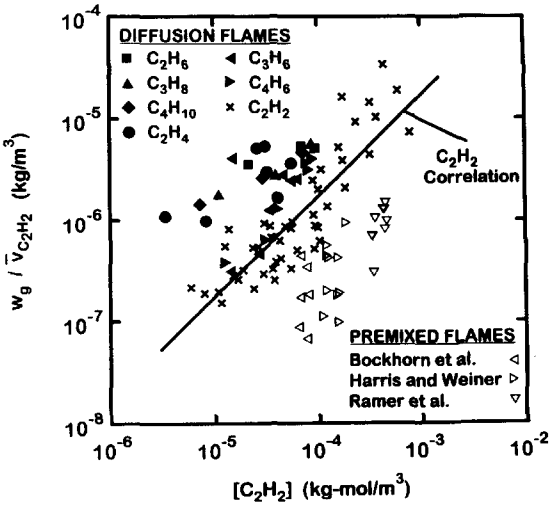

Fig. 14. Net soot growth rates, after correction for soot oxidation, along the axes of laminar hydrocarbon/air diffusion flames, similar results for acetylene/air diffusion flames from Refs. 1 and 2, and gross soot growth rates for premixed flames from Refs. 29–34.

present hydrocarbon/air flames, compared with 0.0030 with an uncertainty (95% confidence) of 0.0006 for the acetylene/air flames [2]. Finally, the oxidation corrections increase the differences between soot growth rates in the diffusion and premixed flames.

The enhancement of net soot growth rates seen in Fig. 14 for the present hydrocarbon/air flames, due to significant concentrations of light hydrocarbons other than acetylene in the soot growth region, will eventually be best treated by detailed models typified by the recent work of Mauss et al. [48] and Kazakov et al. [49], and references cited therein. In particular, such methods will eventually address effects of various species on active soot growth sites and parallel soot growth channels. Nevertheless, present results were interpreted simply in terms of parallel channels, i.e., additive soot growth from various light hydrocarbon species.

The first parallel soot growth mechanism considered assumed that soot growth due to acetylene was unchanged from the correlation of Refs. 1 and 2 (implying an acetylene collision efficiency of 0.0030); and that the residual net soot growth rates were due to ethylene via a collision mechanism represented by Eq. 5. The resulting net growth rates, after accounting for oxidation and for growth due to acetylene (and after eliminating data where oxidation corrections exceeded 50% of the gross soot growth rate), are plotted as a function of ethylene concentration in Fig. 15. The range of

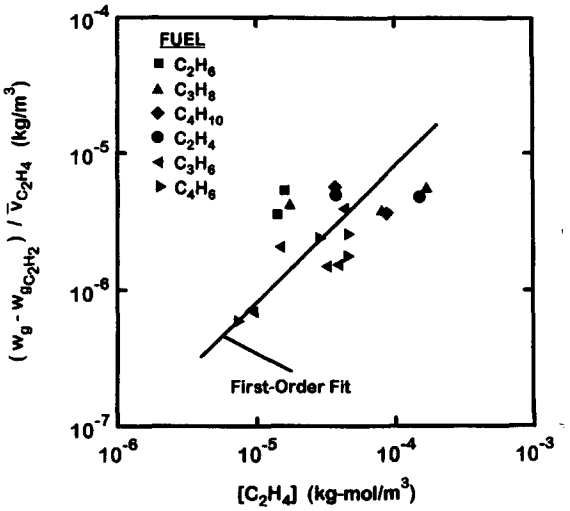

Fig. 15. Net soot growth rates, after correction for soot oxidation and soot growth from acetylene, along the axes of laminar hydrocarbon/air diffusion flames.

ethylene concentrations is too narrow for an accurate determination of the order of the growth rate with respect to ethylene. Instead, the best first-order correlation in terms of ethylene concentration is shown on the plot. The correlation provides a reasonable fit of the measurements, and yields an ethylene collision efficiency of 0.014 with an uncertainty (95% confidence) of 0.005.

Several other mechanisms of soot growth for the hydrocarbon/air flames were considered, involving various parallel growth channels. Table 2 is a summary of the collision efficien-

TABLE 2

Summary of Collision Efficiencies[a]

Mechanism	Flames	$\eta_{C_2H_2}$	$\eta_{C_2H_4}$	η_{CH_4}
C_2H_2	C_2H_2[1, 2]	0.0030[b] (0.0006)	—	—
C_2H_2	present	0.011 (0.004)	—	—
C_2H_2	C_2H_2[1, 2] and present	0.0050 (0.0013)	—	—
C_2H_2/C_2H_4	present	0.0030[b] (–)	0.014 (0.005)	—
C_2H_2/CH_4	present	0.0030[b] (–)	—	0.025 (0.008)
$C_2H_2/C_2H_4/CH_4$	C_2H_2[1, 2] and present	0.0045 (0.0009)	0.00018 (0.002)	0.015 (0.01)

[a] Numbers in parentheses are uncertainties (95% confidence).
[b] Prescribed correlation for laminar acetylene/air flames from Ref. 2.

cies found in this manner, including the following conditions: growth via acetylene for the acetylene/air flames of Refs. 1 and 2; growth via acetylene alone for the present flames as discussed above; growth via acetylene alone for both the acetylene/air flames of Refs. 1 and 2 and the present flames; parallel growth via acetylene and ethylene for the present flames; parallel growth via acetylene and methane for the present flames; and parallel growth via acetylene, ethylene and methane for the acetylene/air flames of Refs. 1 and 2 and the present flames. The first three of these are single-channel mechanisms for various data sets where growth rate is correlated with acetylene concentration without accounting for the presence of other hydrocarbons. The next two are double-channel mechanisms considering ethylene and methane parallel channels, respectively, as discussed above for ethylene. The last mechanism involves a triple channel of acetylene, ethylene and methane and was determined from a three-parameter fit of data from the present flames and from the flames of Refs. 1 and 2. The 4:1 variations of the various collision efficiencies of acetylene for single-channel mechanisms are comparable to changes of surface reactivity attributed to soot growth processes in premixed flames [48, 49]; therefore, effects of surface modification cannot be ruled out. Similarly, the parallel channels yield reasonable collision efficiencies, although the methane channel is not plausible in view of the low H:C ratios of soot, and only yields reasonable collision efficiencies because methane, acetylene, and ethylene concentrations are comparable in the soot growth region. Clearly, consideration of more detailed soot growth mechanisms, and systematic measurements of soot growth within more flame environments, will be required to obtain a more complete treatment of soot growth in flames.

Soot Nucleation

Measurements along the axes of the six test flames were used to study soot nucleation, similar to earlier work [1, 2]. Based on the same assumptions used for soot growth rates in Eq. 2, the expression for soot nucleation rates for motion along a streamline becomes [1]

$$w_n = \rho d(n_p/\rho)/dt. \tag{7}$$

The resulting measurements of w_n are illustrated in Figs. 7–12, along with the concentrations of major hydrocarbon species. These figures show that soot nucleation is associated with the presence of acetylene; indeed, the rates correlate as a first-order acetylene reaction, similar to earlier findings for acetylene/air diffusion flames [1, 2]. This implies

$$w_n = k_n(T)[C_2H_2], \tag{8}$$

where $k_n(T)$ is an Arrhenius expression.

The present soot nucleation rates, expressed in terms of $k_n(T)$ are plotted in Fig. 16. In addition, measured soot nucleation rates from acetylene/air flames from Refs. 1 and 2, and a correlation due to Leung et al. [57] are shown on the plot. The new measurements in hydrocarbon/air diffusion flames are in agreement with the earlier measurements for acetylene/air diffusion flames [1, 2] with the combined results yielding essentially the same first-order

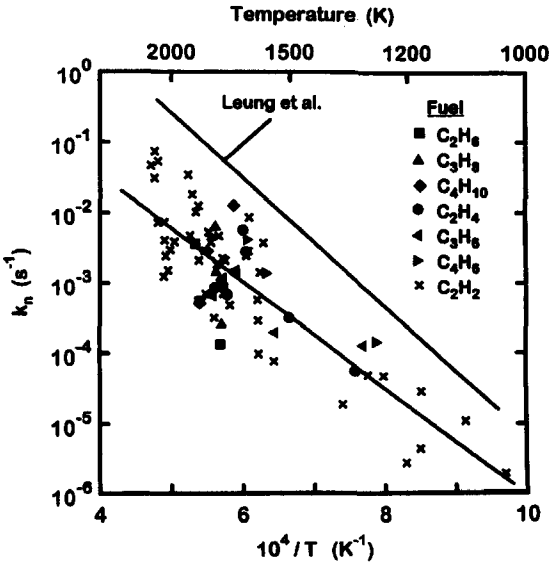

Fig. 16. Soot nucleation rates along the axes of laminar hydrocarbon/air diffusion flames, similar results for acetylene/air diffusion flames from Refs. 1 and 2, and earlier results for soot nucleation rates from Leung et al. [57].

nucleation rate correlation, as follows:

$$w_n = 37.9[C_2H_2]\exp(-17500/T), \quad (9)$$

with w_n (kgmol/m^3/s), $[C_2H_2]$ (kgmol/m^3), and $T(K)$. In Eq. 9, the uncertainty (95% confidence) of the activation temperature is 2680 K, and the correlation coefficient of the fit is 0.84. This implies an activation energy of 35 kcal/gmol, which agrees with the earlier measurements of Ref. 2, within experimental uncertainties. Furthermore, present results indicate that soot nucleation correlates with acetylene concentrations alone, i.e., nucleation does not involve parallel channels, in contrast to soot growth.

As discussed earlier [1, 2], and substantiated by present findings in Fig. 16, present values of w_n are significantly lower than the correlation by Leung et al. [57] of data from various sources. This discrepancy is not surprising, as discussed in Ref. 1. In particular, the data used in Ref. 57 involved questionable optical determinations of primary particle size [36].

Finally, attributing soot nucleation to acetylene alone is an oversimplification of a complex process involving polynuclear aromatic hydrocarbons (PAH) that eventually become visible primary soot particles [5, 48, 49]. Nevertheless, acetylene offers a plausible surrogate for these complex molecules because PAH concentrations can be expressed in terms of acetylene concentrations through equilibrium constants [48, 49]; furthermore, acetylene is a major contributor to the growth of PAH as they evolve toward soot [5].

CONCLUSIONS

Flame structure and soot processes were studied in laminar hydrocarbon/air jet diffusion flames at pressures of 25–99 kPa, emphasizing fuels other than acetylene, in order to supplement earlier findings for laminar acetylene/air jet diffusion flames [1, 2]. Measurements were limited to the axes of the flames where soot first nucleates in the cool core of the flow and experiences a monotonic decrease of mixture fracture along a soot path line. The major conclusions are as follows:

1. Similar to earlier findings for laminar acetylene/air diffusion flames [1, 2], significant soot nucleation and growth began when temperatures reached roughly 1250 K, and where acetylene was detectable, and ended when hydrocarbon concentrations became small (at fuel-equivalence ratios of roughly 1.14). Additionally, relative rates of soot nucleation and growth along the axis combined to yield maximum primary soot particle sizes near the beginning of soot formation, although other paths through diffusion flames can yield different behaviors [2].
2. Present net soot growth rates, corrected for soot oxidation, were larger than earlier observations in acetylene/air diffusion flames, when correlated solely in terms of acetylene concentrations; this behavior is attributed to either parallel soot growth channels due to the presence of light hydrocarbons other than acetylene (ethylene and methane) or modified soot surface reactivity due to the presence of these hydrocarbons. Assuming parallel soot growth channels involving only acetylene and ethylene, and an acetylene collision efficiency of 0.0030 based on earlier measurements in acetylene/air diffusion flames [2], yielded an ethylene collision efficiency of 0.014, although a number of other soot growth mechanisms are discussed as well.
3. In contrast to soot growth rates, present soot nucleation rates agree with earlier observations in laminar acetylene/air diffusion flames [1, 2], and were correlated as a first-order reaction with respect to acetylene with an activation energy of 35 kcal/gmol. The present nucleation rate correlation is significantly lower than the expression suggested by Leung et al. [57]; this difference is attributable to problems, with the approximations used by Leung et al. [57] to estimate soot structure from optical measurements. Finally, it should be recognized that acetylene in the present soot nucleation rate expression serves only as a surrogate for heavier hydrocarbons, e.g., PAH, that eventually evolve to soot. Thus, a more complete treatment of soot nucleation must eventually involve more detailed mechanisms typi-

fied by the methods of Refs. 48 and 49 and references cited therein.

This research was supported by NASA Grant No. NAG3-1245 under the technical management of D. L. Urban of the NASA Lewis Research Center, and the Office of Naval Research Grant No. N00014-93-0321 under the technical management of G. D. Roy.

REFERENCES

1. Sunderland, P. B., Köylü, Ü. Ö., and Faeth, G. M., *Combust. Flame* 100:310–322 (1995).
2. Lin, K.-C., Sunderland, P. B., and Faeth, G. M., *Combust. Flame*, in press.
3. Haynes, B. S., and Wagner, H. Gg., *Prog. Ener. Combust. Sci.* 7:229–273 (1981).
4. Glassman, I., *Twenty-Second Symposium (International) on Combustion*, The Combustion Institute, Pittsburgh, 1988, pp. 295–311.
5. Howard, J. B., *Twenty-Third Symposium (International) on Combustion*, The Combustion Institute, Pittsburgh, 1990, pp. 1107–1127.
6. Kent, J. H., Jander, H., and Wagner, H. Gg., *Eighteenth Symposium (International) on Combustion*, The Combustion Institute, Pittsburgh, 1980, pp. 1117–1126.
7. Kent, J. H., and Wagner, H. Gg., *Combust. Flame* 47:53–65 (1982).
8. Kent, J. H., and Wagner, H. Gg., *Combust. Sci. Technol.* 41:245–269 (1984).
9. Kent, J. H., and Honnery, D. R., *Combust. Flame* 79:287–298 (1990).
10. Honnery, D. R., and Kent, J. H., *Combust. Flame* 82:426–434 (1990).
11. Kent, J. H., and Honnery, D. R., *Combust. Sci. Technol.* 75:167–177 (1991).
12. Honnery, D. R., Tappe, M., and Kent, J. H., *Combust. Sci. Technol.* 83:305–321 (1992).
13. Santoro, R. J., Semerjian, H. G., and Dobbins, R. A., *Combust. Flame* 51:203–218 (1983).
14. Santoro, R. J., Yeh, T. T., Horvath, J. J., and Semerjian, H. G., *Combust. Sci. Technol.* 53:89–115 (1987).
15. Puri, R., Richardson, T. F., Santoro, R. J., and Dobbins, R. A., *Combust. Flame* 92:320–333 (1993).
16. Puri, R., Santoro, R. J., and Smyth, K. C., *Combust. Flame* 97:125–144 (1994); also, Erratum, *Combust. Flame* 102:226–228 (1995).
17. Megaridis, C. M., and Dobbins, R. A., *Twenty-Second Symposium (International) on Combustion*, The Combustion Institute, Pittsburgh, 1988, pp. 353–362.
18. Megaridis, C. M., and Dobbins, R. A., *Combust. Sci. Technol.* 66:1–16 (1989).
19. Dobbins, R. A., Fletcher, R. A., and Lu, W., *Combust. Flame* 100:301–309 (1995).
20. Flower, W. L., and Bowman, C. T., *Combust. Sci. Technol.* 37:93–97 (1984).
21. Flower, W. L., and Bowman, C. T., *Twenty-First Symposium (International) on Combustion*, The Combustion Institute, Pittsburgh, 1986, pp. 1115–1129.
22. Flower, W. L., and Bowman, C. T., *Combust. Sci. Technol.* 53:217–224 (1987).
23. Axelbaum, R. L., Flower, W. L., and Law, C. K., *Combust. Sci. Technol.* 61:51–73 (1988).
24. Axelbaum, R. L., Law, C. K., and Flower, W. L., *Twenty-Second Symposium (International) on Combustion*, The Combustion Institute, Pittsburgh, 1988, pp. 379–386.
25. Vandsburger, U., Kennedy, I. M., and Glassman, I., *Combust. Sci. Technol.* 39:263–285 (1984).
26. Vandsburger, U., Kennedy, I. M., and Glassman, I., *Twentieth Symposium (International) on Combustion*, The Combustion Institute, Pittsburgh, 1984, pp. 1105–1112.
27. Hura, H. S., and Glassman, I., *Combust. Sci. Technol.* 53:1–21 (1987).
28. Hura, H. S., and Glassman, I., *Twenty-Second Symposium (International) on Combustion*, The Combustion Institute, Pittsburgh, 1988, pp. 371–378.
29. Bockhorn, H., Fetting, F., Wannemacher, G., and Wentz, H. W., *Nineteenth Symposium (International) on Combustion*, The Combustion Institute, Pittsburgh, 1982, pp. 1413–1420.
30. Bockhorn, H., Fetting, F., Heddrich, A., and Wannemacher, G., *Twentieth Symposium (International) on Combustion*, The Combustion Institute, Pittsburgh, 1984, pp. 979–988.
31. Harris, S. J., and Weiner, A. M., *Combust. Sci. Technol.* 31:155–167 (1983).
32. Harris, S. J., and Weiner, A. M., *Combust. Sci. Technol.* 32:267–275 (1983).
33. Harris, S. J., and Weiner, A. M., *Combust. Sci. Technol.* 38:75–87 (1984).
34. Ramer, E. R., Merklin, J. F., Sorensen, C. M., and Taylor, T. W., *Combust. Sci. Technol.* 48:241–255 (1986).
35. Gore, J. P., and Faeth, F. M., *Twenty-First Symposium (International) on Combustion*, The Combustion Institute, Pittsburgh, 1986, pp. 1521–1531.
36. Köylü, Ü. Ö., and Faeth, G. M., *J. Heat Transf.* 116:152–159 (1994).
37. Dalzell, W. H., and Sarofim, A. F., *J. Heat Transf.* 91:100–104 (1969).
38. Rosner, D. E., Mackowski, D. W., and Garcia-Ybarra, P., *Combust. Sci. Technol.* 80:87–101 (1991).
39. Sunderland, P. B., Ph.D. dissertation, The University of Michigan, Ann Arbor, Michigan, 1995.
40. Tesner, P. A., *Seventh Symposium (International) on Combustion*, The Combustion Institute, Pittsburgh, 1958, pp. 546–553.
41. Tesner, P. A., *Eighth Symposium (International) on Combustion*, The Combustion Institute, Pittsburgh, 1960, pp. 627–633.
42. Sivathanu, Y. R., and Faeth, G. M., *Combust. Flame* 82:211–230 (1990).

43. Miller, J. H., Honnery, D. R., and Kent, J. H., *Twenty-Fourth Symposium (International) on Combustion*, The Combustion Institute, Pittsburgh, 1992, pp. 1031–1039.
44. Smyth, K. C., Miller, J. H., Dorfman, R. C., Mallard, W. G., and Santoro, R. J., *Combust. Flame* 62:157–181 (1985).
45. Tesner, P. A., *Combust. Flame* 85:279–281 (1991).
46. Tesner, P. A., and Schurupov, S. V., *Combust. Sci. Technol.* 92:61–67 (1993).
47. Tesner, P. A., and Schurupov, S. V., *Twenty-Fifth Symposium (International) on Combustion*, The Combustion Institute, Pittsburgh, 1994, pp. 653–659.
48. Mauss, F., Schäfer, T., and Bockhorn, H., *Combust. Flame* 99:697–705 (1994).
49. Kazakov, A., Wang, H., and Frenklach, M., *Combust. Flame* 100:111–120 (1995).
50. Nagle, J., and Strickland-Constable, R. F., *Proc. Fifth Carbon Conf.* 1:154–164 (1962).
51. Park, C., and Appleton, J. P., *Combust. Flame* 20:369–379 (1973).
52. Johnstone, J. F., Chen, C. Y., and Scott, D. S., *Ind. Eng. Chem.* 44:1564–1569 (1952).
53. Libby, P. A., and Blake, T. R., *Combust. Flame* 36:139–169 (1979).
54. Libby, P. A., and Blake, T. R., *Combust. Flame* 41: 123–147 (1981).
55. Bradley, D., Dixon-Lewis, G., El-Din Habik, S., and Mushi, E. M. J., *Twentieth Symposium (International) on Combustion*, The Combustion Institute, Pittsburgh, 1984, pp. 931–940.
56. Neoh, K. G., Howard, J. B., and Sarofim, A. F., *Particulate Carbon* (D. C. Siegla and B. W. Smith, Eds.), Plenum, New York, 1980, pp. 261–277.
57. Leung, K. M., Lindstedt, R. P., and Jones, W. P., *Combust. Flame* 87:289–305 (1991).

Received 29 November 1994; revised 4 August 1995